Materials Research. 2022; 25:e20210542
DOI: https://doi.org/10.1590/1980-5373-MR-2021-0542

Application of Binary PdSb/C as an Anode in a Polymeric Electrolyte Reactor-Fuel Cell Type for Electrosynthesis of Methanol from Methane

Camila M. Godoi[a], Monique C.L. Santos[a], Livia C. Nunes[a], Araceli J. Silva[a], Andrezza S. Ramos[a], Rodrigo F.B. de Souza[a], Almir O. Neto[a]*

[a]Instituto de Pesquisas Energéticas e Nucleares (IPEN/CNEN-SP), Centro de Célula a Combustível e Hidrogênio (CECCO), Av. Prof. Lineu Prestes, 2422, Cidade Universitária, 05508-900, São Paulo, SP, Brasil.

Received: October 19, 2021; Revised: March 18, 2022; Accepted: April 10, 2022

PdSb catalyst prepared in different compositions were applied as an anode in a polymeric electrolyte reactor - fuel cell type (PER-FC) to convert methane into oxygenated products and energy in mild conditions. The PER-FC polarization curves for $Pd_{90}Sb_{10}/C$ presented maximum current density about 0.92 mW cm^{-2} about 15% higher than PdSb materials. However, the material $Pd_{50}Sb_{50}/C$ showed higher reaction rate for methanol generation than the other materials occurring close to the OCV ($r \sim 7$ mol L^{-1} h^{-1}). The qualitative analyses of PER-FC effluent by FT-IR identified products as methanol, carbonate and formate ions from the partial oxidation of methane for all materials.

Keywords: *Methane into methanol, polymeric electrolyte reactor - fuel cell type, chemical and energy co-generation.*

1. Introduction

Recently, approximately a quarter of the world's energy produced is used to supply the demand of the chemical transformation industry[1,2]. This energy is applied in thermal processes that, although effective, they do not reach maximum efficiency due to the waste of heat caused by the lack of suitable materials and/or reactors that can avoid losses during chemical transformation reactions[3]. In addition, economic, social, legal and environmental organizations put pressure on the research and development area to use the best technological options available so as not to incur high costs so that this energy becomes a resource with low pollution processing.

Therefore, electrochemical processes play an important role, as they act directly on the electrostatic interactions between electron and atomic nucleus through the direct potential application on an atom or molecule, reducing energy losses to the environment[4]. Based on countries willingness to change their primary energy sources to less polluting energy sources, electrochemical processes can gain notoriety and occupy a large space in industrial processes[2].

Nowadays, the industrial processes of partial oxidation of methane occur by converting CH_4 into syngas to be applied in Fischer-Tropsch synthesis, as well a to obtain products such as methanol, formaldehyde, formic acid and other chemicals that are applied as industrial inputs[5,6]. These processes need high temperatures and pressure conditions due to stability CH_4 and it difficult polarization that make it hard to break the C-H bond[3,5,7-9]. However, by electrochemical processes, for example, need to be processed under mild conditions to favor the electrostatic interactions of the molecule of interest[10-12]. The application of electrosynthesis processes increases the yield per unit of energy spent and selectivity[13] unlike traditional thermochemical processes[10-12].

Electrochemical reactors can be built in different ways, one of the most interesting being the electrolytic reactor that uses a solid membrane, capable of reconciling anodic and cathodic reactions, in different chambers of the same device, independently. This makes it possible to associate reactions with energy cogeneration while converting to chemicals[14-17]. In recent years, some studies dealt with the partial oxidation of methane in reactors that use polymeric electrolyte reactor - fuel cell type (PER-FC)[9,18-24], which is still an expanding area. It is known that the application of palladium as a catalyst in these devices favors the production of methanol due to its affinity with methane[18,20,25] having the ability to activate water as the key factor in the transformation of hydrocarbons into oxygenated products. However, the Pd is an expensive and rare metal[26,27].

A strategy to reduce the cost and increase the chemical conversion would be the production of binary materials combining noble metal with other metals or semi-metals with capacity for chemical interaction with methane and/or water activation. The combination of Pd with Sb intensifies the effects of Pd sorption, since the addition of Sb can suppress the CO formation under working conditions in fuel cells[28,29]. Sb-based material have been used in oxidative reaction of methane, as due to the fact that this metal facilitates thermo oxidative coupling[30,31], and presents selective oxidation of methane to formaldehyde that is promoted by the redox cycle of α-Sb_2O_4 and $Sb_2O_4{-}x$[32].

Antimony oxides are widely applied as co-catalysts for various reactions in several applications such as in a fuel cell[30,33,34], due to their ability to activate water, as they are good electrical conductors, interesting for electrocatalysis[35-39].

*e-mail: souza.rfb@gmail.com

This work investigates for the first time the partial oxidation of methane using a PER-FC with binary catalysts based on Pd combined with Sb with different atomic ratios, in alkaline medium, for products and energy co-generation. Therefore this research proposes to make new contributions to the theme.

2. Materials and Methods

For the synthesis of PdSb binary catalytic systems in different atomic compositions, Palladium II Nitrate ($Pd(NO_3)_2.2H_2O$ – Aldrich) and Antimony III Acetate($(CH_3CO_2)_3Sb$ - Aldrich) with 20 wt% of metal loading, were used in this study as metal sources. Sodium Borohydride ($NaBH_4$ – Aldrich) was used as a reducing agent and Vulcan Carbon (XC72) was the support. In the reduction step, the support and the metal sources were dissolved in a mixture of water/2-propanol 50/50 (*v/v*), later the solution content Sodium Borohydride in excess with 10 mL 0.01 mol. L^{-1} of KOH was added. The obtained catalysts were washed with water and dried at 70°C for 2 hours with vacuum filtered.

The synthetized catalysts were characterized by transmission electron microscopy (TEM) and X-ray diffraction (XRD). The micrographs were obtained using a JEOL JEM-2100 electron microscope, operated at 200 Kv. For histogram construction and average size calculation, 300 nanoparticles of each catalyst were averaged digitally. Information on crystalline structures of all catalysts was investigated using the X-ray diffractometer model Miniflex II, with Cukα radiation source of 0.15406Å. Analyses conditions were set at 2θ range 20–90º, with 2 min^{-1} scan speed.

The electrochemical measures via technique of Rotating Ring Disk Electrode (RRDE) were performed using a Parstat 3000A bipotentiostat/galvanostat and an RRDE (Pine Instruments) composed of a gold ring (area = 0.19 cm^2) and a glassy carbon disc (area = 0.25 cm^2) with collection factor of 0.37. In addition, in the conventional electrochemical cell the reference electrode used was Ag/AgCl (3mol L^{-1} KCl) and Pt was used as counter electrode ($area_g$ = 2 cm^2). The working electrodes was prepared with 15 µL aliquot of each previously prepared paint composed of a mixture of 8 mg of each catalyst + 750 µl of H_2O, 250 µl of isopropyl alcohol and 15 µl of 5% Nafion D-520. All experiments with different catalysts were performed in 1mol L^{-1} KOH medium. The curves were obtained at different speeds ranging from 100, 400, 600, 900, 1600 and 2500 rpm with potential range of 0.2 V - -0.85 V, and v = 10 mV s^{-1}. Ring was polarized at 0.2 V.

For perform in PER-FC tests, the membrane electrode assembly (MEA) was made with a *Nafion*® 117 membrane treated with KOH per 48 hours, Pt/C BASF catalyst (20% by weight) with 1 mg cm^{-2} as cathode in gas diffusion electrodes; and catalysts with different PdSb ratios (20 wt%) as anode. All electrodes were prepared by painting the Nafion soaked catalyst ink, over a PTFE treated carbon cloth. The ink was previously prepared using the dry electrocatalyst and a 5% in mass of Nafion D-520 solution (Aldrich). The reactor, a cell with ElectroChem unit-type serpentine distribution, was supplied with CH_4 at a flow rate of 100 mL min^{-1} and 1.0 molL^{-1} KOH at a flow rate of 1 mL min^{-1} at room temperature at the anode and external O_2 with the temperature controlled humidifier bottle at 85°C with a flow of 400 ml min^{-1} in the cathode.

The Fourier Transform Infrared (FTIR) spectroscopy technique was used to identify the different species formed during the electrochemical oxidation of methane in alkaline medium at different potentials. Anodic reaction products were collected by 300s increments of 50 mV and analyzed by ATR-FTIR performed on an ATR accessory (MIRacle with a ZnSe Crystal Plate Pike®) installed on a Nicolet® 6700 FT-IR spectrometer equipped with a cooled MCT detector with N_2 liquid. The quantification of methanol was developed by Boyaci's method with Raman spectroscopy[20,40], using Horiba Scientific MacroRam Raman spectroscopy equipment, set at 785 nm wavelength.

3. Results and Discussion

Figure 1 shows the x-ray diffractograms of PdSb materials supported on carbon. The peak near to 25º was attributed to carbon (JCPDF # 50-926) for all materials. Analyzing the materials containing Pd it is possible to observe peaks about 2θ ≈ 40º, 47º, 68º, 82º and 87º associated, respectively, to (111), (200), (220), (311) and (222) planes of Pd (JCPDS # 89-4897) with face-centered cubic (FCC) structure. With the increase in the amount of antimony in the catalyst, the peaks will lose resolution. Narrower and more defined peaks appear, indicating an improvement in the crystallographic structure of the structure present by the noble metal.

In the diffractogram of the Sb/C is possible to observe peaks at ≈ 27º, 31º, 45º and 55º relative to the Sb_2O_3 phase (JCPDS # 5-534), the peak 27º being apparent in the diffractograms of materials $Pd_{80}Sb_{20}$, $Pd_{70}Sb_{30}$, $Pd_{60}Sb_{40}$ and

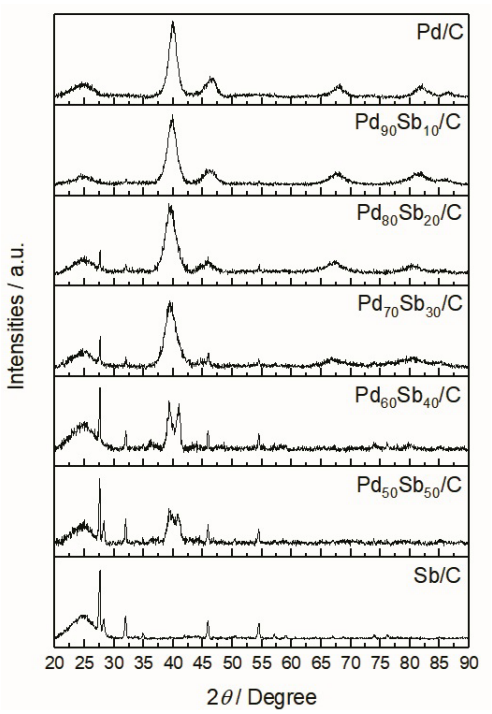

Figure 1. X-ray diffractograms of PdSb/C catalysts and different compositions.

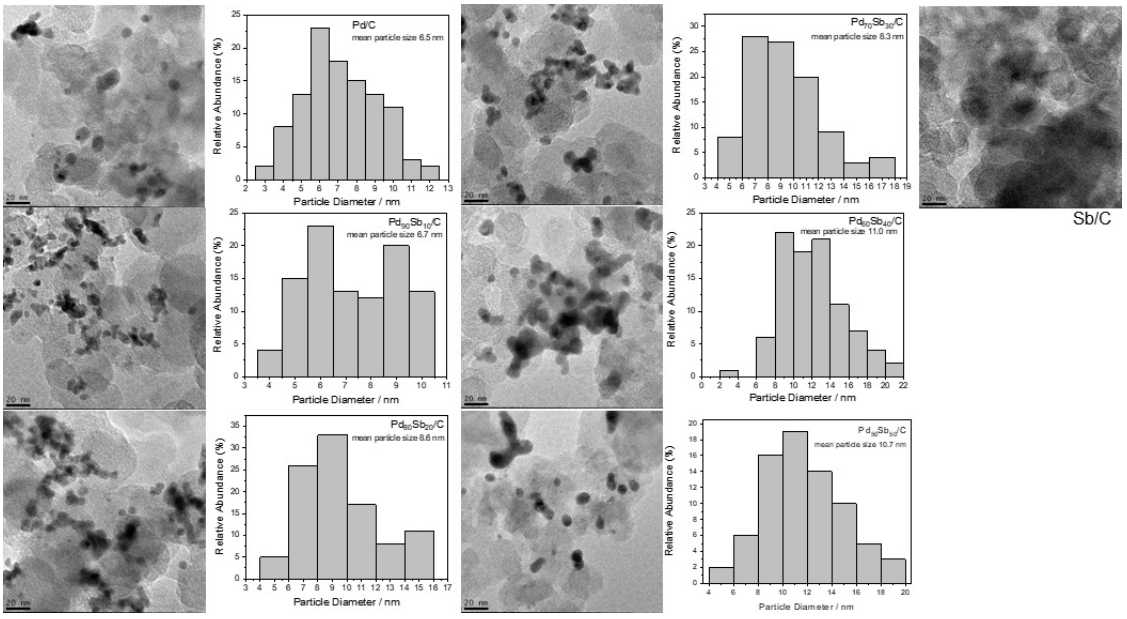

Figure 2. Micrographs obtained by TEM and distribution histograms of PdSb/C materials in different compositions.

$Pd_{50}Sb_{50}$. The peak at ≈ 28° observed in Sb/C and $Pd_{50}Sb_{50}$/C can be associated to Sb (JCPDS # 85-1322). The $Pd_{60}Sb_{40}$/C and $Pd_{50}Sb_{50}$/C catalysts still show a peak at 41° that can be attributed to the Pd_8Sb_3 phase (JCPDS # 30-95) with rhombohedra structure, which does not interfere with peak 220 of Pd at 68°, observed also by Yu and Pickup[41]. However, the materials $Pd_{80}Sb_{20}$/C and $Pd_{70}Sb_{30}$/C presents the peak ≈ 68 shifted to less positive values, indicating an expansion in the Pd network parameter by inserting Sb atoms.

TEM images of the PdSb catalysts (Figure 2) were observed, in materials synthesized with a high amount of Pd, a good dispersion with some regions of agglomerations in the Vulcan XC72 support, in catalysts with increased Sb precursor, the average particle size and the amount of agglomerates show increasing behavior, which refers to the Sb_2O_3 phase[42]. The mean particle sizes are 6.5 nm for Pd/C, 6.7 nm for $Pd_{90}Sb_{10}$/C, 8.6 nm for $Pd_{80}Sb_{20}$/C, 8.3 nm for $Pd_{70}Sb_{30}$/C, 11 nm for $Pd_{60}Sb_{40}$/C, 10.7 nm for $Pd_{50}Sb_{50}$/C and for Sb/C does not possible to account due the high agglomeration, which may also be due to the ripening effect[43], where smaller particles with greater surface energy favour the dissolution in larger particles.This result explains the low resolution of Pd peak observed in XRD measures, and is in agreement of the literature[35,44].

Figure 3 present the cyclic voltammetry pattern obtained for PdSb electrocatalysts in alkaline media, is possible to observe the region of adsorption/desorption of hydrogen on Pd (- 0.85V to -0.45V).The increase of Sb amount showed an increase in the current values in the double layer (-0.45 – 0.15 V) in relation to Pd/C, which may be attributed to the formation of antimony species[35,45]. For $Pd_{70}Sb_{30}$/C, $Pd_{60}Sb_{40}$/C, $Pd_{50}Sb_{50}$/C and Sb/C materials with current close to -0.18V is possible to see a peak, may be attributed to the change of oxidation state of Sb[46], similar peak is observed for $Pd_{80}Sb_{20}$, however shifted for 70 mV more negative (-0.25V) probably due to the phase difference observed by XRD measurements.

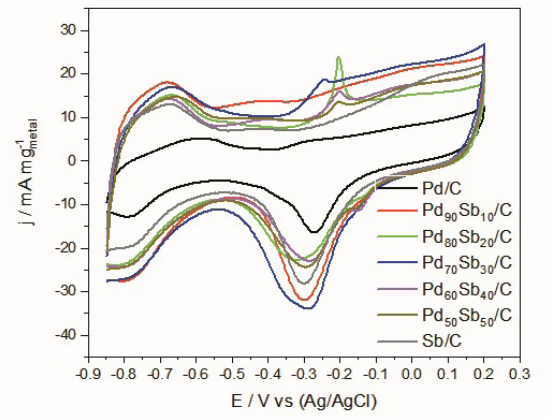

Figure 3. Cyclic voltammetry of PdSb materials in KOH 1 mol.L^{-1} (v= 10 mV.s^{-1})

The fundamental step for the oxidation of methane by electrochemical ways is the activation of water that generates hydroxyl radicals which in turn promote the breaking of the C-H bond[26,27,47,48], in agreement with Equations 1 and 2.

$$H_2O + MO \rightarrow MOH + OH\bullet \quad (1)$$

$$CH_4 + OH\bullet \rightarrow CH_3OH \quad (2)$$

Garcia et al.[49] to detect indirectly the these oxygenated radicals use the rotation ring disk experiments to measure the H_2O_2 or in its deprotonated form due to the alkaline medium HO_2^{-1} in alkaline media, as an Equation 3[50]:

$$\bullet OH + \bullet OH \rightarrow HO_2^{-1} \quad (3)$$

To evaluate the ability of PdSb/C materials to perform this step, rotating ring disk measurements were made. In Figure 4 the results of RRDE curves for HO_2^{-1} generation and detection process reveals that the highest currents measured for HO_2^{-1} detection correspond to materials with the highest amounts of Sb ($Pd_{50}Sb_{50}$/C, $Pd_{60}Sb_{40}$/C and Sb/C), being that the material Sb/C presented a current three times greater than the second most active material during the whole potential range. The richest materials in Pd (Pd/C and $Pd_{90}Sb_{10}$/C) compose the second group formed by the most active materials. However the materials $Pd_{80}Sb_{20}$/C and $Pd_{70}Sb_{30}$/C, that presented greater distortions in the Pd FCC structure few amount of HO_2^{-1}, indicating that these materials can operate in a 4 electron mechanism to reduce oxygen in accordance with the literature[46].

The measurement of hydrogen peroxide detection current is relative to the tested electrodes, however the relationship between the disc and ring currents may indicate which material is preferred for the H_2O_2 generation mechanism. The selectivity for the formation of peroxide (% H_2O_2) can be calculated by Equation 4[51]:

$$H_2O_2\% = \frac{200 I_r / N}{I_d + I_r / N} \quad (4)$$

Where I_d is the disk current, I_r is the ring current, and N is the RRDE collection efficiency (0.37). The calculated results are showed in Figure 5, where the H_2O_2% lines in the potential range from -0.8 V to -0.0 V, and the mean H_2O_2 production~ 20, ~5%, ~4%, ~4%, ~3%, ~1% and ~0.6% for Sb/C, $Pd_{60}Sb_{40}$/C, $Pd_{50}Sb_{50}$/C,Pd/C, $Pd_{90}Sb_{10}$/C, $Pd_{80}Sb_{20}$/C, and $Pd_{70}Sb_{30}$/C respectively.

Figure 6 presents the polarization curves of polymeric electrolyte reactor - fuel cell type for PdSb/C materials with KOH and methane fed on the anode. The maximum current density measured was 0.22 mA cm^{-2}, 0.16 mA cm^{-2}, 0.154 mA cm^{-2}, 0.149 mA cm^{-2}, 0.12 mA cm^{-2}, 0.11mA cm^{-2}, 0.09 mA cm^{-2} respectively for$Pd_{90}Sb_{10}$/C, $Pd_{70}Sb_{30}$/C, Pd/C, $Pd_{80}Sb_{20}$/C, $Pd_{50}Sb_{50}$/C, $Pd_{60}Sb_{40}$/C, and Sb/C. The OCV obtained is close than reported in the literature for methane oxidation at mild conditions using SER-FC (about 0.3 -0.4V)[9,18,20,23,52].

The SER-FC effluent was collected for qualitative and quantitative measures. Figure 7 shows IR spectra of partial oxidation products. The bands at 1482 cm^{-1} for CH_3 d-deform[53], 1080 cm^{-1} and 1030 cm^{-1} [19,20] confirm the methanol production over PdSb materials.

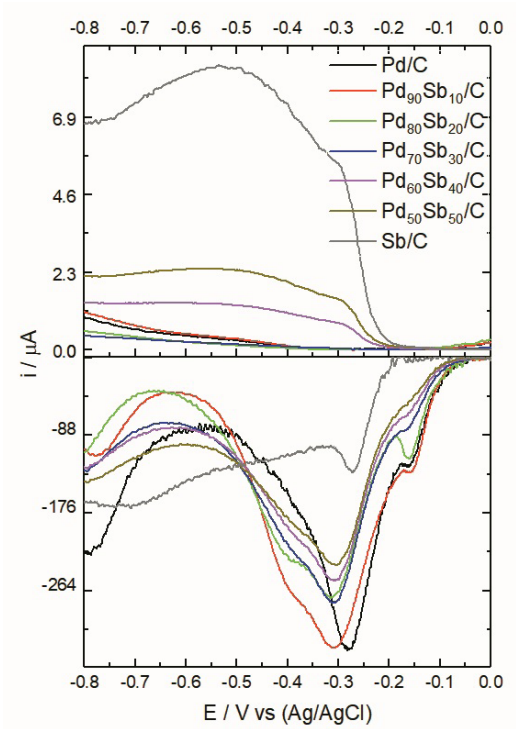

Figure 4. RRDE voltammograms at 1600 r.p.m. in O_2saturated electrolyte with the disc current with v = 10 mV s^{-1}, ring current (polarized at 0.2V) corresponding to hydrogen peroxide detection.

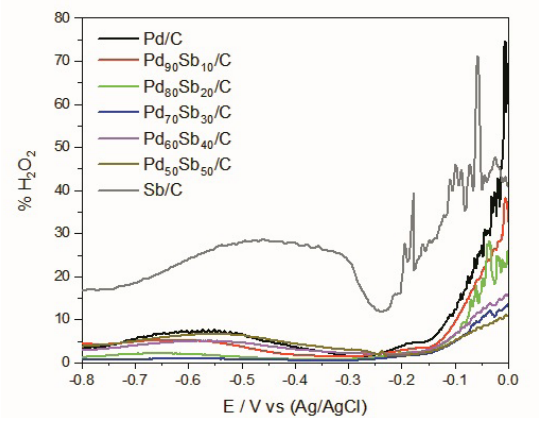

Figure 5. H_2O_2% selectivity as a function of the applied potential.

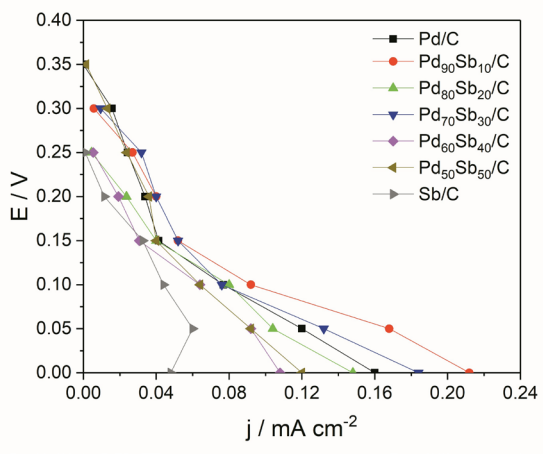

Figure 6. Polarization curves of a 5 cm^2 SER-FC at room temperature using PdSb/C catalysts anodes (1mg_{metal} cm^{-2} catalyst loading) and Pt/C Basf for the cathode in all experiments (1mg_{Pt} cm^{-2} catalyst loading with 20 wt% Pt loading on carbon), Nafion 117 membrane KOH treated KOH 1.0 $molL^{-1}$ + CH_4 50 $mL.min^{-1}$, and O_2 flux of 400 mL min^{-1}.

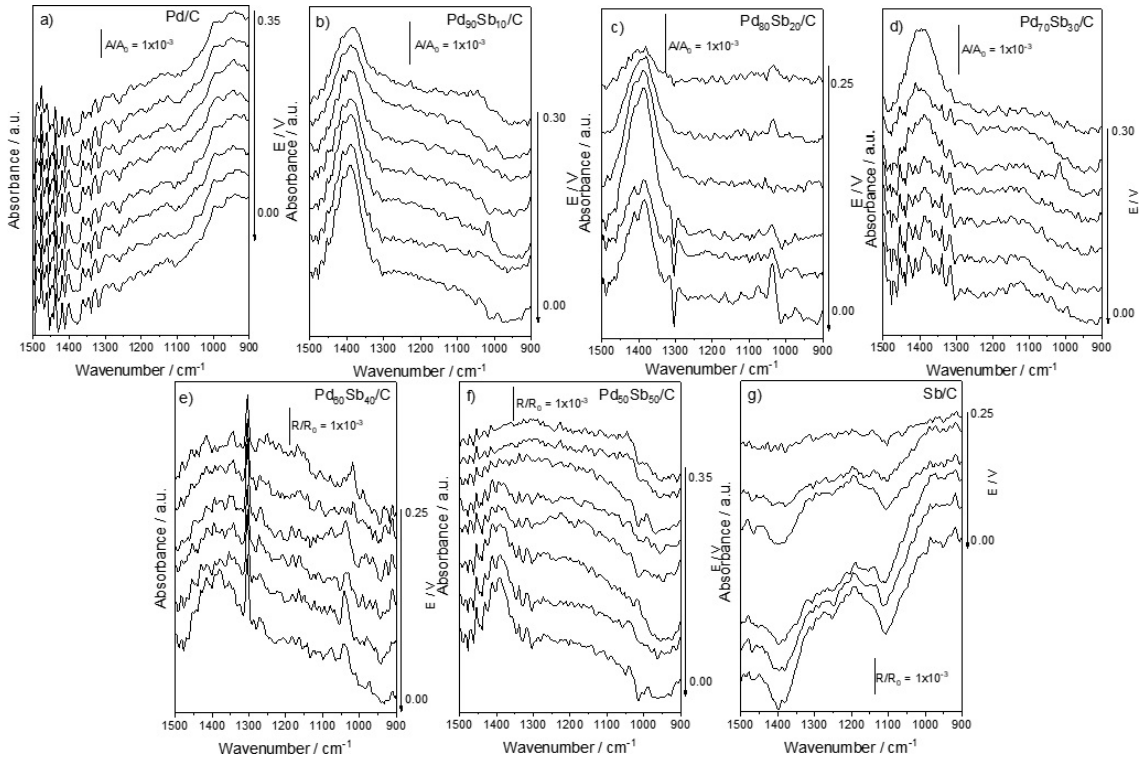

Figure 7. FTIR spectra were taken from effluent of SER-FC at several potentials in 1.0 mol.L^{-1} KOH and the methane flow was set to 50 mL.min^{-1}.

The band at 1030 cm^{-1}, observed in all materials, increases with decreasing reactor potential. However, this band is not as selective as the band-centered ≈ 1080 cm^{-1} that appears differently for each material. For Pd/C and $Pd_{80}Sb_{20}$/C this band was already observed in the OCV values and presents few changes in intensity up to zero V. For $Pd_{90}Sb_{10}$/C this same band increases in intensity with the reduction of the reactor potential up to 0.05 V, then, after this potential, the band decreases. For $Pd_{70}Sb_{30}$/C, this band is very close to the signal/noise and it was not possible describe its behavior. $Pd_{60}Sb_{40}$/C and $Pd_{50}Sb_{50}$/C shows an increasing behavior due to the potential decrease. Sb/C is observed only between 0.15 V and 0.05 V. The band at 1478 cm^{-1} is only observed for Sb/C due to the absence of interference from the band related to carbonate ions (~1376 cm^{-1}), products of complete oxidation of the methane observed for all materials containing Pd, indicating the complete methane oxidation also occur[54,55]. Complete oxidation can occur in stages, as confirmed by the presence of methanol during the potential variation. If this alcohol is present in greater quantity, when it is oxidized, the OCV increases. This fact may justify the OVC value higher than that observed in the literature.

The band centered at 1345 cm^{-1}that correspond to ν(COO) of formate solution[56],it is present only for $Pd_{70}Sb_{30}$/C. The formate is probably due to methanol oxidation reaction, more evidently observed in $Pd_{60}Sb_{40}$/C and $Pd_{50}Sb_{50}$/C, indicating that those compositions can promote higher methane oxidation than others. The band centered at ~ 1302 cm^{-1} correspond to deg deform of methane[52,57] and it is observed in all materials. This signal increase may be due to the increase of methane solubility in solution[20].

The quantitative measures was based according to Boyaci's method[40]. To calculate the methanol production by the reaction rate (r) expressed in Equation 5. The analytical curve was constructed in the concentration range of 0.005-1.000 mol.L^{-1} of methanol. For the following analytical curve, an intensity = 3.3509 + 3.983 [methanol] is obtained with the correlation coefficient being 0.97.

$$r = \frac{Methanol_{amount}}{Volume\,x\,Time} \quad (5)$$

The calculated r for each potential are shown in Figure 8. The materialsPd/C, $Pd_{90}Sb_{10}$/C, $Pd_{60}Sb_{40}$/C and $Pd_{50}Sb_{50}$/C produce methanol in appreciable quantities at all potentials. The higher r was obtained with $Pd_{50}Sb_{50}$/C (r ~ 7 mol L^{-1} h^{-1}), occurring close to the OCV, and with Pd/C (~ 6.75 mol L^{-1} h^{-1} at 0.2V). These materials showed selective generation of H_2O_2 around 4 and 5% and convert methane into methanol in all potentials, selectivity similar to reported by Garcia[49] for more active materials for conversion of methane into methanol using copper complex. Indicating that reaction cam be depend heavily on an optimal amount of reactive oxygenated species to maximize conversion of methane into methanol.

The materials $Pd_{80}Sb_{20}$/C and $Pd_{70}Sb_{30}$/C present relevant quantities only between 0.3V to 0.1V and in lesser quantities than the others. This result is in accordance with the selectivity results to H_2O_2 generation (Figure 4). Although Sb/C

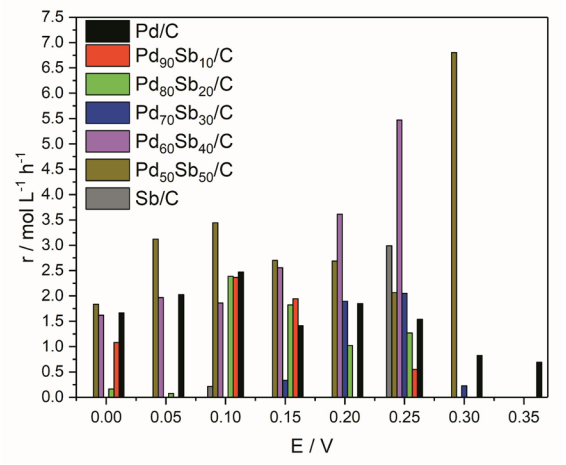

Figure 8. Methanol concentration obtained for PdSb / C materials and proportions.

presents more selective for H_2O_2, practically no methanol was detected. This can be explained by i) the loading and unloading process due to the reversible reactions of the alloy characteristic of elementary Sb which are further impaired by the superficial passivation of Sb[58], ii) due to the high population of oxygenated reactive species, produced by the activation of water, the reaction are leading to more oxidized products, and/or iii) even with the high activity for generation of reactive species, the lack of methane adsorption sites hinder methanol conversion. While Pd catalysts were more selective for methanol, mainly those that presented higher selectivity values for H_2O_2. Results previously published by several groups on the study of kinetics and energetic interactions in PdO in relation to methane show that the formation of a thin layer of PdO on the electrocatalyst surface to obtain the necessary binding effect is responsible for decreasing the initial C-H bond in methane[20,25,59,60]. The addition of antimony to Pd enhances the effect described with greater abundance of oxygenated reactive species.

4. Conclusion

PdSb materials synthesized by the $NaBH_4$ method were active for the conversion of methane into products with energy co-generation on a PER-FC, the main products being potassium formate and methanol, however, the selectivity and efficiency depending of the composition and the phases present in the material that can change the way the reaction proceeds. For Pd/Cand $Pd_{90}Sb_{10}$/C the Pd FCC is practically not altered by the addition of Sb, presents a selectivity of 3 to 4% for H_2O_2 and conversion of methane to methanol in all potentials. $Pd_{80}Sb_{20}$ and $Pd_{70}Sb_{30}$ the lattice parameter of Pd is expanded by the insertion of Sb atoms in the FCC structure, practically not selective to generating H_2O_2 (0.6% to 1%) and has limited conversion of methanol to the potential range of 0.6 to 0.2V. $Pd_{60}Sb_{40}$ and $Pd_{50}Sb_{50}$ present in addition to the FCC structure for Pd, also present in dominant form the structure rhombohedra phase Pd_8Sb3. These materials showed selective generation of H_2O_2 around 4 and 5% and convert methane into methanol in all potentials. These binary catalysts have proven to be more efficient than the Pd/C catalyst itself, in addition to a higher power density, due to the production of more oxidized derivatives, such as potassium formate. Sb/C, despite being more selective for the generation of H_2O_2, there is a lack of an interaction system between methane and the catalyst. This behavior increases the conversion of hydrocarbon to alcohol. In other words, the activation of water, although essential for the partial oxidation of methane, is not the only characteristic necessary for the conversion of this hydrocarbon into oxygenated products by means of a PER-FC.

5. Acknowledgments

We are grateful to CAPES (88882.315566/2019), CNPq (302709/2020-7), FAPESP (2017/11937-4), and CINE-SHELL (ANP)/FAPESP grants 2017/11937-4 for financial supports.

6. References

1. Orella MJ, Román-Leshkov Y, Brushett FR. Emerging opportunities for electrochemical processing to enable sustainable chemical manufacturing. Curr Opin Chem Eng. 2018;20:159-67.
2. Blanco DE, Modestino MA. Organic electrosynthesis for sustainable chemical manufacturing. Trends in Chemistry. 2019;1(1):8-10.
3. Nimkar SC, Mewada RK, Rosen MA. Exergy and exergoeconomic analyses of thermally coupled reactors for methanol synthesis. Int J Hydrogen Energy. 2017;42(47):28113-27.
4. Yan M, Kawamata Y, Baran PS. Synthetic organic electrochemical methods since 2000: on the verge of a renaissance. Chem Rev. 2017;117(21):13230-319.
5. Xie S, Lin S, Zhang Q, Tian Z, Wang Y. Selective electrocatalytic conversion of methane to fuels and chemicals. J Energy Chem. 2018;27(6):1629-36.
6. Shi D, Liu J, Sun R, Ji S, Rogers SM, Connolly BM, et al. Preparation of bifunctional Au-Pd/TiO2 catalysts and research on methanol liquid phase one-step oxidation to methyl formate. Catal Today. 2018;316:206-13.
7. San-José-Alonso D, Juan-Juan J, Illán-Gómez MJ, Román-Martínez MC. Ni, Co and bimetallic Ni–Co catalysts for the dry reforming of methane. Appl Catal A Gen. 2009;371(1):54-9.
8. Shavi R, Hiremath V, Seo JG. Radical-initiated oxidative conversion of methane to methanol over metallic iron and copper catalysts. Molecular Catalysis. 2018;445:232-9.
9. Lee B, Hibino T. Efficient and selective formation of methanol from methane in a fuel cell-type reactor. J Catal. 2011;279(2):233-40.
10. Zakaria Z, Kamarudin SK. Direct conversion technologies of methane to methanol: an overview. Renew Sustain Energy Rev. 2016;65:250-61.
11. Rocha RS, Reis RM, Lanza MRV, Bertazzoli R. Electrosynthesis of methanol from methane: the role of V2O5 in the reaction selectivity for methanol of a TiO2/RuO2/V2O5 gas diffusion electrode. Electrochim Acta. 2013;87:606-10.
12. Dhiman SS, Shrestha N, David A, Basotra N, Johnson GR, Chadha BS, et al. Producing methane, methanol and electricity from organic waste of fermentation reaction using novel microbes. Bioresour Technol. 2018;258:270-8.
13. Blanco DE, Lee B, Modestino MA. Optimizing organic electrosynthesis through controlled voltage dosing and artificial intelligence. Proc Natl Acad Sci USA. 2019;116(36):17683-9.
14. Mohammed H, Al-Othman A, Nancarrow P, Tawalbeh M, El Haj Assad M. Direct hydrocarbon fuel cells: A promising technology for improving energy efficiency. Energy. 2019;172:207-19.

15. Zhou Z-Y, Wang Q, Lin J-L, Tian N, Sun S-G. In situ FTIR spectroscopic studies of electrooxidation of ethanol on Pd electrode in alkaline media. Electrochim Acta. 2010;55(27):7995-9.
16. De Souza RFB, Silva JCM, Simoes FC, Calegaro ML, Neto AO, Santos MC. New Approaches for the Ethanol Oxidation Reaction of Pt/C on Carbon Cloth Using ATR-FTIR. Int J Electrochem Sci. 2012;7(6):5356-66.
17. Qian Q-Y, Yang C, Zhou Y-G, Yang S, Xia X-H. Efficient C–C bond cleavage in ethanol electrooxidation on porous Pt catalysts. J Electroanal Chem. 2011;660(1):57-63.
18. Nandenha J, Nagahama I, Yamashita J, Fontes E, Ayoub J, de Souza R, et al. Activation of methane on PdZn/C electrocatalysts in an acidic electrolyte at low temperatures. Int J Electrochem Sci. 2019;14:10819-34.
19. Nandenha J, Piasentin RM, Silva LMG, Fontes EH, Neto AO, de Souza RFB. Partial oxidation of methane and generation of electricity using a PEMFC. Ionics. 2019;25(10):5077-82.
20. Santos MCL, Nunes LC, Silva LMG, Ramos AS, Fonseca FC, de Souza RFB, et al. Direct alkaline anion exchange membrane fuel cell to converting methane into methanol. Chemistry Select. 2019;4(39):11430-4.
21. Tomita A, Nakajima J, Hibino T. Direct oxidation of methane to methanol at low temperature and pressure in an electrochemical fuel cell. Angew Chem Int Ed. 2008;47(8):1462-4.
22. Ma M, Jin BJ, Li P, Jung MS, Kim JI, Cho Y, et al. Ultrahigh electrocatalytic conversion of methane at room temperature. Adv Sci. 2017;4(12):1700379.
23. Lee B, Sakamoto Y, Hirabayashi D, Suzuki K, Hibino T. Direct oxidation of methane to methanol over proton conductor/metal mixed catalysts. J Catal. 2010;271(2):195-200.
24. Spinner N, Mustain WE. Electrochemical methane activation and conversion to oxygenates at room temperature. J Electrochem Soc. 2013;160(11):F1275-81.
25. Stotz H, Maier L, Boubnov A, Gremminger AT, Grunwaldt JD, Deutschmann O. Surface reaction kinetics of methane oxidation over PdO. J Catal. 2019;370:152-75.
26. Boyd MJ, Latimer AA, Dickens CF, Nielander AC, Hahn C, Nørskov JK, et al. Electro-Oxidation of Methane on Platinum under Ambient Conditions. ACS Catal. 2019;9(8):7578-87.
27. Arnarson L, Schmidt PS, Pandey M, Bagger A, Thygesen KS, Stephens IEL, et al. Fundamental limitation of electrocatalytic methane conversion to methanol. Phys Chem Chem Phys. 2018;20(16):11152-9.
28. Haan JL, Stafford KM, Masel RI. Effects of the addition of antimony, tin, and lead to palladium catalyst formulations for the direct formic acid fuel cell. J Phys Chem C. 2010;114(26):11665-72.
29. Haan JL, Stafford KM, Morgan RD, Masel RI. Performance of the direct formic acid fuel cell with electrochemically modified palladium–antimony anode catalyst. Electrochim Acta. 2010;55(7):2477-81.
30. Lo MY, Agarwal SK, Marcelin G. Oxidative coupling of methane over antimony-based catalysts. J Catal. 1988;112(1):168-75.
31. Agarwal SK, Migone RA, Marcelin G. Oxidative coupling of methane over alkali-doped antimony oxide. Appl Catal. 1989;53(1):71-80.
32. Matsumura H, Okumura K, Shimamura T, Ikenaga N-o, Miyake T, Suzuki T. Selective oxidation of methane to formaldehyde over antimony oxide-loaded catalyst. J Mol Catal Chem. 2006;250(1):122-30.
33. Binions R, Carmalt CJ, Parkin IP. Antimony oxide thin films from the atmospheric pressure chemical vapour deposition reaction of antimony pentachloride and ethyl acetate. Polyhedron. 2006;25(15):3032-8.
34. van Steen E, Schnobel M, Walsh R, Riedel T. Time on stream behaviour in the partial oxidation of propene over iron antimony oxide. Appl Catal A Gen. 1997;165(1):349-56.
35. Ayoub JMS, Geraldes AN, Tusi MM, Spinace EV, Neto AO. Preparation of PtSnSb/C by an alcohol reduction process for direct ethanol fuel cell (DEFC). Ionics. 2011;17(6):559-64.
36. Marshall AT, Haverkamp RG. Electrocatalytic activity of IrO2–RuO2 supported on Sb-doped SnO2 nanoparticles. Electrochim Acta. 2010;55(6):1978-84.
37. Piasentin RM, de Souza RFB, Silva JCM, Spinacé EV, Santos MC, Neto AO. Electro-oxidation of Ethanol on PtPdSn/C-Sb2O5. SnO2 electrocatalysts prepared by borohydride reduction. Int J Electrochem Sci. 2013;8(1):435-45.
38. Neto AO, Brandalise M, Dias RR, Ayoub JMS, Silva AC, Penteado JC, et al. The performance of Pt nanoparticles supported on Sb2O5.SnO2, on carbon and on physical mixtures of Sb2O5. SnO2 and carbon for ethanol electro-oxidation. Int J Hydrogen Energy. 2010;35(17):9177-81.
39. Frolova L, Lyskov N, Dobrovolsky Y. Nanostructured Pt/SnO2–SbOx–RuO2 electrocatalysts for direct alcohol fuel cells. Solid State Ion. 2012;225(0):92-8.
40. Boyaci IH, Genis HE, Guven B, Tamer U, Alper N. A novel method for quantification of ethanol and methanol in distilled alcoholic beverages using Raman spectroscopy. J Raman Spectrosc. 2012;43(8):1171-6.
41. Yu X, Pickup PG. Deactivation resistant PdSb/C catalysts for direct formic acid fuel cells. Electrochem Commun. 2010;12(6):800-3.
42. Chin HS, Cheong KY, Abdul Razak K. Effect of process parameters on size, shape, and distribution of Sb2O3 nanoparticles. J Mater Sci. 2011;46(15):5129-39.
43. Segets D, Martinez Tomalino L, Gradl J, Peukert W. Real-time monitoring of the nucleation and growth of ZnO nanoparticles using an optical hyper-rayleigh scattering method. J Phys Chem C. 2009;113(28):11995-2001.
44. Geraldes AN, Da Silva DF, Pino ES, Da Silva JCM, De Souza RFB, Hammer P, et al. Ethanol electro-oxidation in an alkaline medium using Pd/C, Au/C and PdAu/C electrocatalysts prepared by electron beam irradiation. Electrochim Acta. 2013;111:455-65.
45. Rodrigues da Silva M, Ângelo ACD. Synthesis and Characterization of Ordered Intermetallic Nanostructured PtSn/C and PtSb/C and Evaluation as Electrodes for Alcohol Oxidation. Electrocatalysis. 2010;1(2):95-103.
46. Xu J, Aili D, Li Q, Pan C, Christensen E, Jensen JO, et al. Antimony doped tin oxide modified carbon nanotubes as catalyst supports for methanol oxidation and oxygen reduction reactions. J Mater Chem A Mater Energy Sustain. 2013;1(34):9737-45.
47. Nidheesh PV, Zhou M, Oturan MA. An overview on the removal of synthetic dyes from water by electrochemical advanced oxidation processes. Chemosphere. 2018;197:210-27.
48. Santos MCL, Godoi CM, Kang HS, de Souza RFB, Ramos AS, Antolini E, et al. Effect of Ni content in PdNi/C anode catalysts on power and methanol co-generation in alkaline direct methane fuel cell type. J Colloid Interface Sci. 2020;578:390-401.
49. Garcia LMS, Rajak S, Chair K, Godoy CM, Silva AJ, Gomes PVR, et al. Conversion of methane into methanol using the [6,6′-(2,2′-Bipyridine-6,6′-Diyl)bis(1,3,5-Triazine-2,4-Diamine)](Nitrato-O)Coppe r(II) complex in a solid electrolyte reactor fuel cell type. ACS Omega. 2020;5(26):16003-9.
50. Nogami G, Nishiyama Y, Nakamura H. New approach to a rotating ring disk electrode. J Electrochem Soc. 1988;135(4):877-84.
51. Zhou R, Zheng Y, Jaroniec M, Qiao S-Z. Determination of the electron transfer number for the oxygen reduction reaction: from theory to experiment. ACS Catal. 2016;6(7):4720-8.
52. Nandenha J, Fontes EH, Piasentin RM, Fonseca FC, Neto AO. Direct oxidation of methane at low temperature using Pt/C, Pd/C, Pt/C-ATO and Pd/C-ATO electrocatalysts prepared by sodium borohydride reduction process. J Fuel Chem Technol. 2018;46(9):1137-45.

53. Tsuchida E, Kanada Y, Tsukada M. Density-functional study of liquid methanol. Chem Phys Lett. 1999;311(3):236-40.
54. Fang X, Wang L, Shen PK, Cui G, Bianchini C. An in situ Fourier transform infrared spectroelectrochemical study on ethanol electrooxidation on Pd in alkaline solution. J Power Sources. 2010;195(5):1375-8.
55. Fontes EH, Piasentin RM, Ayoub JMS, da Silva JCM, Assumpção MHMT, Spinacé EV, et al. Electrochemical and in situ ATR-FTIR studies of ethanol electro-oxidation in alkaline medium using PtRh/C electrocatalysts. Mater Renew Sustain Energy. 2015;4(1)
56. Christensen PA, Linares-Moya D. The role of adsorbed formate and oxygen in the oxidation of methanol at a polycrystalline pt electrode in 0.1 M KOH: an in situ fourier transform infrared study. J Phys Chem C. 2010;114(2):1094-101.
57. Scarano D, Bertarione S, Spoto G, Zecchina A, Otero Areán C. FTIR spectroscopy of hydrogen, carbon monoxide, and methane adsorbed and co-adsorbed on zinc oxide. Thin Solid Films. 2001;400(1):50-5.
58. Zhao X, Vail SA, Lu Y, Song J, Pan W, Evans DR, et al. Antimony/graphitic carbon composite anode for high-performance sodium-ion batteries. ACS Appl Mater Interfaces. 2016;8(22):13871-8.
59. Kinnunen NM, Hirvi JT, Suvanto M, Pakkanen TA. Role of the Interface between Pd and PdO in Methane Dissociation. J Phys Chem C. 2011;115(39):19197-202.
60. Weaver JF, Hakanoglu C, Antony A, Asthagiri A. Alkane activation on crystalline metal oxide surfaces. Chem Soc Rev. 2014;43(22):7536-47.